2CroCEE
22 - 24 March 2023

Proceedings of the 2nd Croatian Conference on Earthquake Engineering - 2CroCEE
Zagreb, Croatia - March 22 to 24, 2023

DOI: https://doi.org/10.5592/CO/2CroCEE.2023.3

POWER RESPONSES OF A BUILDING UNDER THE EXCITATION OF PULSE-LIKE GROUND MOTIONS

Jui-Liang Lin [(1)]

[(1)] *Research Fellow, National Center for Research on Earthquake Engineering, Taipei, Taiwan, jllin@narlabs.org.tw*

Abstract

In comparison with far-field (FF) ground motions, near-fault (NF) ground motions with forward directivity or fling-step effect are characterized by large pulses. These pulse-like (PL) ground motions have pronounced coherent pulses in velocity and displacement histories. Even though these prominent pulses generally have very few cycles in a PL ground motion, the destruction they cause to structures is severe and distinctive compared with non-pulse-like (NPL) ground motions. The present study suggests power demand as an alternative engineering demand parameter for reflecting the severity of the risk posed by PL ground motions. The proposed parameter is simply a product of story shears and inter-story velocities. Through an investigation using a three-story building subjected to ensembles of PL and NPL ground motions, this study confirms that power demand satisfactorily elucidates the destructive potential of PL ground motions. In contrast, force demand, which is the cornerstone laid in building seismic design codes, cannot adequately reflect the destructive potential of PL ground motions. In addition to power, power density and normalized power density were introduced to obtain a sense of the magnitude of power demand relative to the degree of structural damage.

From the energy response histories of a three-story building, extraordinary increments of kinetic energy under a PL ground motion are closely followed by significant increments of strain energy, indicating large structural deformations. It was found that damping energy is not effectively built up at the first significant increment of strain energy. This implies that inherent or supplemental damping hardly protects building structures against the first crucial strike of PL ground motions, which usually cause the most damage to structures.

Keywords: near-fault ground motion, power response, seismic response, velocity pulse, vertically irregular building

1. Introduction

In comparison with far-field (FF) ground motions, near-fault (NF) ground motions with forward directivity or fling-step effect are characterized by large pulses [1-4]. These pulse-like (PL) ground motions have pronounced coherent pulses in velocity and displacement histories. Even though these prominent pulses generally have very few cycles in a PL ground motion, the destruction they cause to structures is severe and distinctive compared with non-pulse-like (NPL) ground motions.

Kalkan and Kunnath [4] demonstrated that the velocity pulse of an NF ground motion causes structures to dissipate considerable input energy in relatively few large deformation cycles. They questioned the validity of the process of amplifying elastic design spectra with NF factors to reflect NF effects, which is commonly stipulated in design codes [5]. They also pointed out that the maximum inter-story drift ratio is a function of the ratio of pulse period to fundamental structural period. The study concluded that acceleration and velocity response spectra should be collectively examined to rationally assess the damage potential of NF ground motions [4]. Through conducting incremental dynamic analyses (IDA), Sehhati et al. [6] showed that neither the PGA nor the spectral acceleration corresponding to the first-mode period are an ideal intensity measure (IM) for capturing structural responses to PL ground motions. They found that the PGV seems to be the only IM valid for both NF and FF ground motions. Enderami et al. [7] showed that the hysteretic energy caused by FF ground motions increases gradually, whereas in NF ground motions most hysteretic energy occurs in the first two yield excursions. This was believed to be the main difference between the effects of FF and NF ground motions on structures. Accordingly, they proposed an energy-based pushover analysis approach to estimate the NF ground

DOI: https://doi.org/10.5592/CO/2CroCEE.2023.3

motion-induced seismic demands of structures [7]. Recognizing that structural seismic damage is associated with input energy and the ability of structural components to dissipate energy, Kalkan and Kunnath [8] proposed an energy measure to correlate with peak seismic demands. That energy measure is defined as the energy demand imposed on a structure over an effective duration, namely the time between two zero-crossings of the effective velocity pulse.

Because many densely populated cities of Taiwan are near active faults, the seismic responses of a three-story reinforced concrete (RC) building (Fig. 1) to NF ground motions were investigated through a shaking table test [9]. The three-story building was vertically irregular, with a soft bottom story due to an elevated first story and additional RC walls only on the two exterior sides of the third story. The three-story building purposely mimicked many existing buildings, where the first stories are elevated and used for stores or parking lots; the other stories with many partition walls are used for residences. The numerical model of the three-story building was satisfactorily calibrated and verified with experimental results [9]. By performing IDA on the numerical model, it was found that when the building is collapsed, the total input energy from an amplified NF ground motion record was approximately half of that from an amplified FF ground motion record. This finding demonstrated that the amount of input energy is not a measure that appropriately reflects the potential damage caused by NF ground motions. Moreover, a notable two-sided spike with almost equal positive and negative displacement magnitudes was observed when the amplified NF ground motion collapsed the building. Meanwhile, the kinetic energy of the building, which reflects structural velocity, drastically increased [9]. This observation suggests that outstanding structural velocity accompanying a prominent structural displacement (i.e., a large restoring force) is one of the characteristics of buildings responding to NF ground motions, compared with FF ground motions. It is thus reasonable to infer that great power demands are imposed on buildings under NF ground motions.

A useful analogy is that the work done by an adult carrying a 30 kg object up three stories in ten minutes is the same as that done in ten seconds, whereas the power demand in the latter case is 60 times the power demand of the former case. It is reasonable to presume that the former case is achievable, or even simple, for an ordinary adult, but most adults would be hard pressed or unable to achieve the second effort. Another analogy is to consider two identical steel boxes, one containing coals, the other bombs. Assuming that the energy dissipated by burning the coals and exploding the bombs are equal, the degree of damage is expected to be substantially different because of the discrepancy between the power, rather than the energy imposed on the two boxes. Accordingly, it seems intuitive and desirable to distinguish the threats of PL and NPL ground motions to buildings by examining their respective induced power demands. The present study therefore examines the power responses of the validated numerical model of the abovementioned three-story building to PL and NPL ground motions. The results are expected to provide a window into the understanding of the distinctive threat to buildings under PL ground motions.

(a)

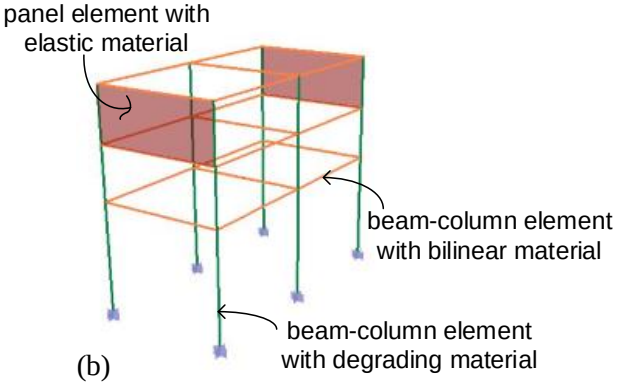

(b)

Figure 1. a) The three-story RC building (the white part) on an 8 m × 8 m shaking table; b) the numerical model.

Proceedings of the 2nd Croatian Conference on Earthquake Engineering - 2CroCEE
Zagreb, Croatia - March 22 to 24, 2023

DOI: https://doi.org/10.5592/CO/2CroCEE.2023.3

2. Power responses of a three-story building

Power response, denoted by $P(t)$, of an N-story building is defined as:

$$P(t) = \sum_{i=1}^{N} P_i(t) = \sum_{i=1}^{N} h_i \theta_i'(t) V_i(t) \tag{1}$$

where $P_i(t)$, h_i, and $V_i(t)$ are the power, story height, and story shear of the ith story, respectively. Parameter $\theta_i'(t)$ is the time derivative of the ith inter-story drift ratio $\theta_i(t)$. Thus, $h_i\theta_i'(t)$ represents the inter-story velocity of the ith story. Under a ground motion excitation, both $V_i(t)$ and $\theta_i'(t)$, of an elastic building structure vary linearly as the ground motion intensity (e.g., PGA) varies. Consequently, the power response is a quadratic function in terms of the ground motion intensity (Eq. 1).

2.1 Numerical model

To maintain the integrity of the present paper but avoid duplications, the details of the three-story building [9] are supplied in Appendix A. In addition to the elastic panel elements for simulating the RC walls, the numerical model of the three-story building consists of beam-column elements for simulating the beams and columns. A degrading material capable of reflecting strength degradation, stiffness degradation, and pinching is used for the columns. A bilinear material is adopted for the beams, and all the floor slabs are assumed to be rigid diaphragms. The calibration and verification of the numerical model have been conducted through shaking table tests, in which the three-story building went into a significant inelastic excursion with a peak inter-story drift of 2.49% rad [9]. The shaking table tests also confirmed that the building had a first-mode vibration period (T_1) of 0.395 s in the short direction (i.e., x-direction). The effective modal participation mass ratio of the first vibration mode is 98.63%. The first vibration mode thus overwhelmingly dominates the seismic vibrations of the building, whose deformation is concentrated in the soft bottom story. Moreover, Rayleigh damping, with the damping ratios of the first two x-directional vibration modes equal 3%, is used to represent the inherent damping of the building [9].

2.2 Selected ground motion records

The present numerical study considers an ensemble of 19 PL ground motion records and an ensemble of 19 NPL ground motion records. All the selected records were from seismic events in Taiwan. Ten records in each ensemble are from the 1999 Chi-Chi earthquake, which created an abundance of PL ground motion records. Table 1 shows the details of the selected PL and NPL records. The identification of ground motions with PL velocities is based on the wavelet approach proposed by Shahi and Baker [10]. The ground motion is classified as PL when the proposed pulse indicator is positive and the pulses arrive early in the time history. Moreover, the period associated with the maximum Fourier amplitude of the extracted wavelet, also known as the pseudoperiod of the wavelet, is estimated as the pulse period T_p [10]. Figure 2a–2f illustrates the 5%-damped displacement response spectra (S_d), pseudo-velocity response spectra (PS_v), and pseudo-acceleration response spectra (PS_a) of the two ground motion record ensembles. Figure 2a–2f clearly shows that PL records generally have greater spectral values at medium and long periods compared with NPL records. Figure 2g–2i plots the PL and NPL medians of S_d, PS_v, and PS_a to facilitate comparison. It should also be noted that four PL records (No. 2, 5, 6, and 7 in Figure 2a and 2b) possess outstanding S_d and PS_v values at medium and long periods. With all the selected ground motion records applied in the x-direction of the building, the IDA [11] were carried out. The pseudo-spectral acceleration at the first-mode period, denoted by $S_a(T_1)$, was used as the IM, and was scaled from 0.15 g to 3.0 g with increments of 0.15 g. With the IDA results, it was found that No. 9 of the PL records and No. 6 of the NPL records (CHY080_EW listed in Table 1a and TCU076_NS listed in Table 1b) resulted in the most significant seismic demands, which will be addressed in the following section. Besides the PL and NPL medians, the spectra of PL No. 9 and NPL No. 6 are also illustrated in Figure 2g–2i. Figure 2g–2i clearly indicates that all the PL medians of S_d, PS_v, and PS_a at the first-mode period (T_1 = 0.395 s) are lower than their NPL counterparts. The PS_v and PS_a of PL No. 9 at the first-mode period are also lower than their counterparts of NPL No. 6, whereas their S_d values are

Proceedings of the 2nd Croatian Conference on Earthquake Engineering - 2CroCEE
Zagreb, Croatia - March 22 to 24, 2023

DOI: https://doi.org/10.5592/CO/2CroCEE.2023.3

essentially equal. Moreover, the median PL PS_a has a substantial and wider plateau, compared with the NPL median. The median PL PS_v has an outstanding ridge at a period of one-second, whereas the median NPL PS_v is not obviously ridge-shaped.

Table 1 – Ensembles of selected (a) PL and (b) NPL ground motion records.

(a)

GM No.	EQ Event	Magnitude (M_w)	Station	Component	R_{rup} (kM)	V_{s30} (m/s)	Duration (s)	T_p (s)
1	1999_ChiChi	7.65	CHY006	EW	9.158	422.68	100	2.57
2	1999_ChiChi	7.65	CHY101	NS	9.150	252.37	90	5.34
3	1999_ChiChi	7.65	TCU045	NS	26.060	706.96	90	9.33
4	1999_ChiChi	7.65	TCU047	EW	35.095	522.97	90	12.31
5	1999_ChiChi	7.65	TCU052	EW	1.040	589.22	90	12.29
6	1999_ChiChi	7.65	TCU065	EW	0.176	290.11	90	5.74
7	1999_ChiChi	7.65	TCU068	EW	0.429	490.00	90	12.29
8	1999_ChiChi	7.65	TCU095	EW	45.076	454.10	90	8.69
9	1999_ChiChi	6.3	CHY080	EW	22.398	499.17	90	1.38
10	1999_ChiChi	6.19	TCU084	EW	15.919	733.78	34	1.44
11	1999_Chiayi	5.86	CHY073	EW	7.549	201.48	90	1.13
12	2006_Taitung	6.17	TTN027	EW	9.104	318.22	71	1.27
13	2010_Jiaxian	6.29	CHY063	EW	4.806	287.66	103	1.16
14	2013_Nantou	6.01	TCU143	EW	23.626	465.91	75	1.27
15	2013_Nantou	6.3	TCU167	EW	14.518	363.85	83	1.19
16	2016_Meinong	6.4	CHY062	EW	21.519	597.85	80	0.90
17	2016_Meinong	6.4	CHY063	EW	16.829	287.66	106	1.44
18	2016_Meinong	6.4	CHY089	NS	19.013	396.20	120	2.58
19	2018_Hualien	6.4	HWA028	NS	0.900	404.91	120	4.17

GM = ground motion, EQ = earthquake; R_{rup} is the distance from the station to the ruptured fault; V_{S30} is the average shear-wave velocity at depths between 0 and 30 m.

(b)

GM No.	EQ Event	Magnitude (M_w)	Station	Component	R_{rup} (kM)	V_{s30} (m/s)	Duration (s)
1	1994_Nanao	6.35	ILA031	EW	13.758	657.39	90
2	1999_ChiChi	7.65	CHY028	NS	2.049	546.91	90
3	1999_ChiChi	7.65	CHY041	NS	19.411	488.12	90
4	1999_ChiChi	7.65	TCU071	NS	5.793	614.75	90
5	1999_ChiChi	7.65	TCU072	EW	6.731	471.88	90
6	1999_ChiChi	7.65	TCU076	NS	1.945	573.23	90
7	1999_ChiChi	7.65	TCU078	EW	8.664	444.54	90
8	1999_ChiChi	7.65	TCU079	EW	11.401	353.94	90
9	1999_ChiChi	7.65	TCU084	NS	11.714	733.78	90
10	1999_ChiChi	7.65	TCU129	EW	0.990	506.46	90
11	1999_ChiChi	6.3	TCU078	EW	7.768	444.54	105
12	1999_Chiayi	5.86	CHY035	EW	17.814	554.22	68
13	1999_Chiayi	5.57	CHY106	EW	17.092	227.63	94
14	2003_Taitung	6.83	TTN041	EW	24.718	431.59	186
15	2003_Taitung	6.83	TTN042	NS	14.340	824.52	186
16	2003_Taitung	6.83	TTN046	EW	15.200	529.10	183
17	2010_Jiaxian	6.29	CHY047	EW	45.941	183.52	80
18	2016_Meinong	6.4	CHY061	EW	19.917	499.94	82
19	2018_Hualien	6.4	HWA051	NS	—	449.74	104

Proceedings of the 2nd Croatian Conference on Earthquake Engineering - 2CroCEE
Zagreb, Croatia - March 22 to 24, 2023

DOI: https://doi.org/10.5592/CO/2CroCEE.2023.3

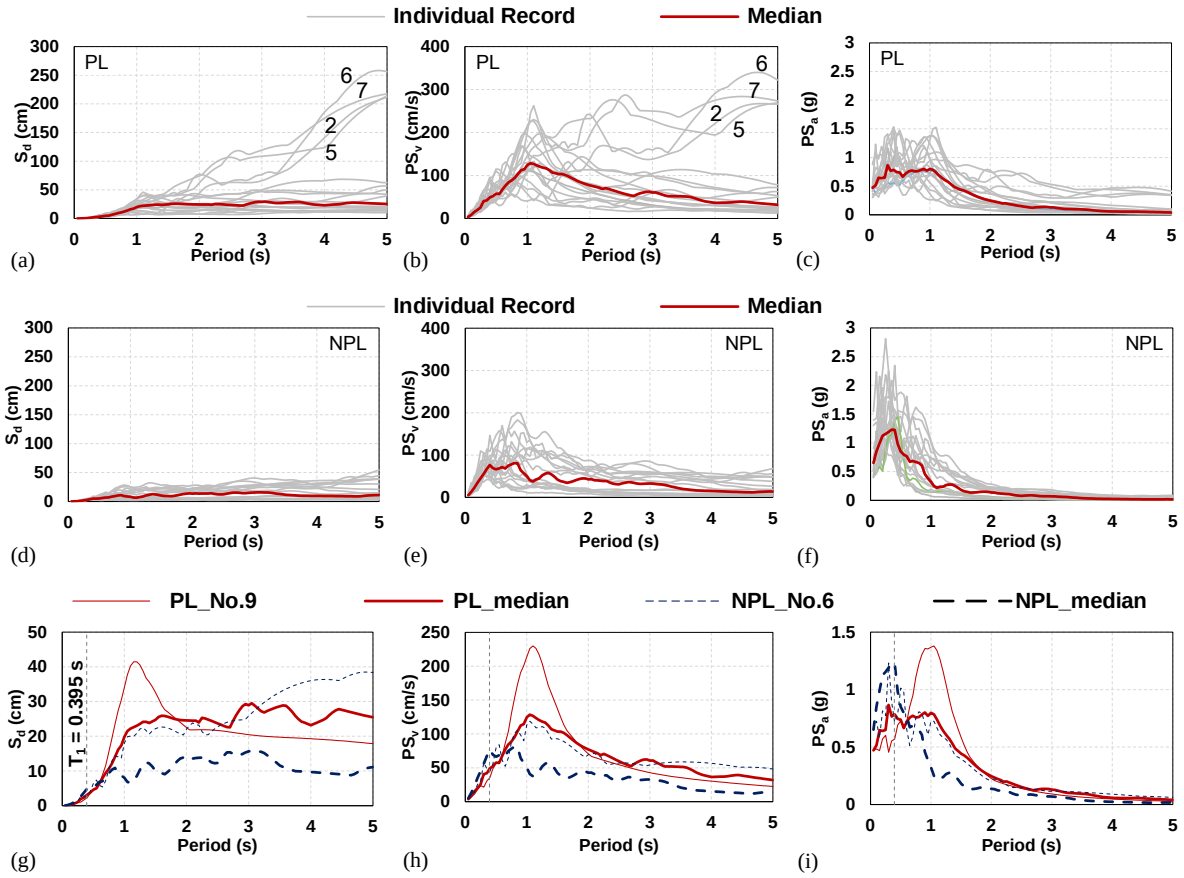

Figure 2. (a) S_d, (b) PS_v, and (c) PS_a PL response spectra; (d) S_d, (e) PS_v, and (f) PS_a NPL response spectra; (g) S_d, (h) PS_v, and (i) PS_a response spectra of PL No. 9, NPL No. 6, PL median, and NPL median.

3. Seismic responses to ensembles of ground motion records

Fig. 3a–3d illustrates the peak values of the inter-story drift, inter-story velocity, story shear, and story power of the first story (denoted by $\theta_{1,\text{peak}}$, $h_1\theta'_{1,\text{peak}}$, $V_{1,\text{peak}}$, and $P_{1,\text{peak}}$, respectively) when the three-story building is subjected to the PL ground motions (No. 1 to 19 in Table 1a). The value of h_1 is 300 cm (Fig. A1). Fig. 3e–3h represents the counterparts when the building is subjected to the NPL ground motions (No. 1 to 19 in Table 1b). In each plot of Fig. 3, there are twenty lines or layers, each of which is the structural response corresponding to a certain value of $S_a(T_1)$, which varies from 0.15 g to 3.0 g with increments of 0.15 g. The value of $S_a(T_1)$ essentially increases from the bottom line to the top line. In fact, Fig. 3 shows few crossings between different lines. This phenomenon reflects "structural resurrection", which means that a greater IM ($S_a(T_1)$) results in less structural response [11]. Comparing the ordinates of Fig. 3a–3d with Fig. 3e–3h indicates that, except for $V_{1,\text{peak}}$, the seismic responses ($\theta_{1,\text{peak}}$, $h_1\theta'_{1,\text{peak}}$, and $P_{1,\text{peak}}$) resulting from the PL records are noticeably greater than those resulting from the NPL records when $S_a(T_1)$ approaches 3.0 g. This indicates that force demand is not an appropriate measure for distinguishing the seismic risks posed by PL and NPL ground motions. In other words, structural damage caused by PL ground motions is more likely to be due to power demand or velocity demand. Further, compared with inter-story velocity demand, power demand seems to be a physical quantity that is more straightforward and explicit for representing destructive potential of PL ground motions.

Because of structural softening, Fig. 3a clearly shows that the spacing between layers with greater values of $S_a(T_1)$ is generally and noticeably larger than that for lower values of $S_a(T_1)$. In contrast, because of the gradually saturated story shear, Fig. 3c shows that the spacing between the layers with greater values of $S_a(T_1)$ is generally less than that compared with smaller values of $S_a(T_1)$. As $S_a(T_1)$

Proceedings of the 2nd Croatian Conference on Earthquake Engineering - 2CroCEE
Zagreb, Croatia - March 22 to 24, 2023

DOI: https://doi.org/10.5592/CO/2CroCEE.2023.3

increases, curves in Fig. 3a, 3b, and 3d are strikingly alike, whereas those in Fig. 3e, 3f, and 3h are not as alike as their PL counterparts. Speaking in detail, there are four outstanding peaks in each of Fig. 3a, 3b, and 3d, which correspond to the No. 5/6, 9/10, 12/13, and 17 PL ground motions, and which are not necessarily the same as the four ground motion records with outstanding S_d and PS_v values shown in Fig. 2a and b (No. 2, 5, 6, and 7). Furthermore, the magnitude sequence from large to small of the four peaks in Fig. 3a, 3b, and 3d are identical (No. 9/10, 5/6, 17, and 12/13). As for the NPL records, there are seven outstanding peaks in Fig. 3e, 3f, and 3h. The seven peaks correspond to No. 2, 4, 6, 8, 11, 13, and 18 NPL ground motions. Nevertheless, the magnitude sequence of the seven peaks is rather inconsistent. These observations again confirm that power demand is an effective measure that reflects the damage potential of PL ground motions. However, the effectiveness decreases when power demand is used as a measure for reflecting the damage potential of NPL ground motions. In other words, power demand plays a critical role in the seismic damage to buildings under PL ground motions, which usually only exhibit two or three extraordinarily large excursions in the corresponding hysteretic loops. In contrast, in the seismic damage to buildings under NPL ground motions, where gradually increasing hysteretic loops (i.e., cumulative damage) are more common, power demand is not as crucial.

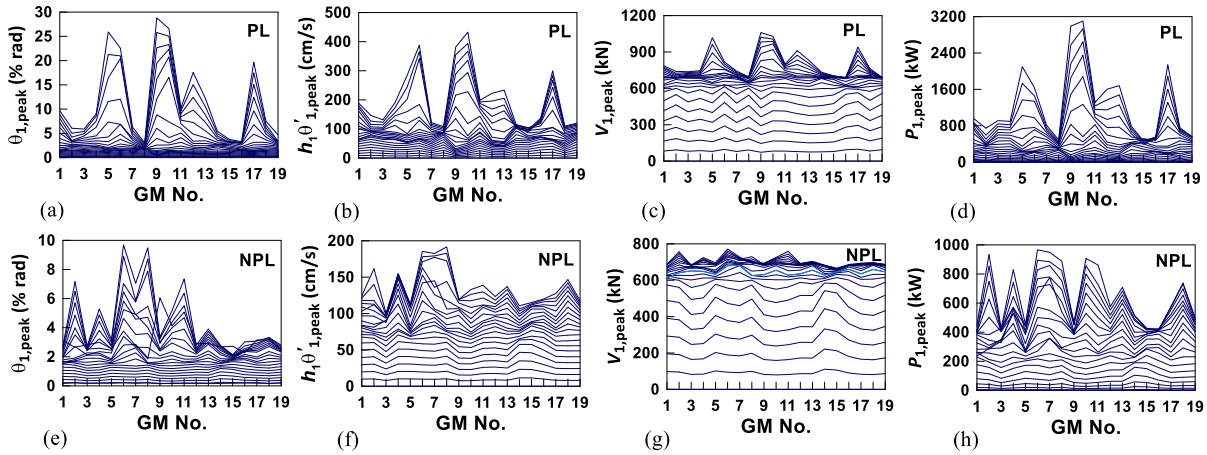

Figure 3. (a) $\theta_{1,\text{peak}}$, (b) $h_1\theta'_{1,\text{peak}}$, (c) $V_{1,\text{peak}}$, and (d) $P_{1,\text{peak}}$ of the three-story building subjected to the PL ground motions scaled from $S_a(T_1)$ = 0.15 g to 3.0 g; (e)–(h) are the counterparts of (a)–(d) subjected to the NPL ground motions.

Fig. 4a–4d shows the IDA curves of $\theta_{1,\text{peak}}$, $h_1\theta'_{1,\text{peak}}$, $V_{1,\text{peak}}$, and $P_{1,\text{peak}}$ for the three-story building under the PL excitations. The 16%, 50% (median), and 84% percentiles of the IDA curves are shown together. Fig. 4e–4h shows the counterparts under the NPL excitations. Comparison of these graphs indicates that the PL ground motions impose greater seismic threats to the building than the NPL ground motions. In addition, the variation in seismic demand among the PL ground motions is more significant than among the NPL ground motions. For clarity, Fig. 4i–4l compares the medians of the $\theta_{1,\text{peak}}$, $h_1\theta'_{1,\text{peak}}$, $V_{1,\text{peak}}$, and $P_{1,\text{peak}}$ IDA curves resulting from the two ground motion record ensembles. Fig. 4i and 4k indicates that the building is essentially elastic when $S_a(T_1)$ is less than 1.0 g. Note that the first vibration mode of the building overwhelmingly dominates the seismic vibrations [9]. Therefore, as long as the ground motion records are scaled to an identical pseudo-spectral acceleration $S_a(T_1)$, i.e., $(2\pi/T_1)^2 S_d(T_1)$, the elastic drift response $\theta_{1,\text{peak}}$ (Fig. 4a, 4e, and 4i) of the building is mostly unvaried from ground motion to ground motion. On the other hand, the values of $h_1\theta'_{1,\text{peak}}$, $V_{1,\text{peak}}$, and $P_{1,\text{peak}}$ are much more diverse from ground motion to ground motion even when the building is elastic (Fig. 4b–4d and 4f–4h). This phenomenon possibly results from varying spectral values of $h_1\theta'_{1,\text{peak}}$, $V_{1,\text{peak}}$, and $P_{1,\text{peak}}$ among ground motion records, although all the ground motion records are scaled to an identical $S_a(T_1)$. In addition, higher-mode effects may be more substantial in these three types of seismic responses ($h_1\theta'_{1,\text{peak}}$, $V_{1,\text{peak}}$, and $P_{1,\text{peak}}$) compared with $\theta_{1,\text{peak}}$.

Proceedings of the 2nd Croatian Conference on Earthquake Engineering - 2CroCEE
Zagreb, Croatia - March 22 to 24, 2023

DOI: https://doi.org/10.5592/CO/2CroCEE.2023.3

When the building is elastic ($S_a(T_1) \leqq 1.0$ g), the quadratic variation of $P_{1,peak}$ (Fig. 4l) appears unique in comparison with the linear variations of $\theta_{1,peak}$, $h_1\theta'_{1,peak}$, and $V_{1,peak}$ (Fig. 4i–4k). Moreover, the $h_1\theta'_{1,peak}$ and $P_{1,peak}$ of the building responding to the PL ground motions are initially lower but eventually much greater than their NPL counterparts (Fig. 4j and 4l). As the seismic intensity of the PL ground motion increases, the rapidly increased $P_{1,peak}$ poses a severe threat to the building (Fig. 4l). This threat is clearly reflected in the median $\theta_{1,peak}$ of the building in response to the PL ground motions, which remarkably surpasses its NPL counterpart as the $S_a(T_1)$ gradually approaches 3.0 g (Fig. 4i). In contrast, the discrepancy between the maximum base shears, i.e., the peak first story shears ($V_{1,peak}$), resulting from the PL and NPL ground motions (Fig. 4k) is not so significant in comparison with the discrepancy between the corresponding $\theta_{1,peak}$ medians (Fig. 4i) when $S_a(T_1) = 3.0$ g. This phenomenon indicates that force demand is not adequate for differentiating the seismic risks posed by PL and NPL ground motions.

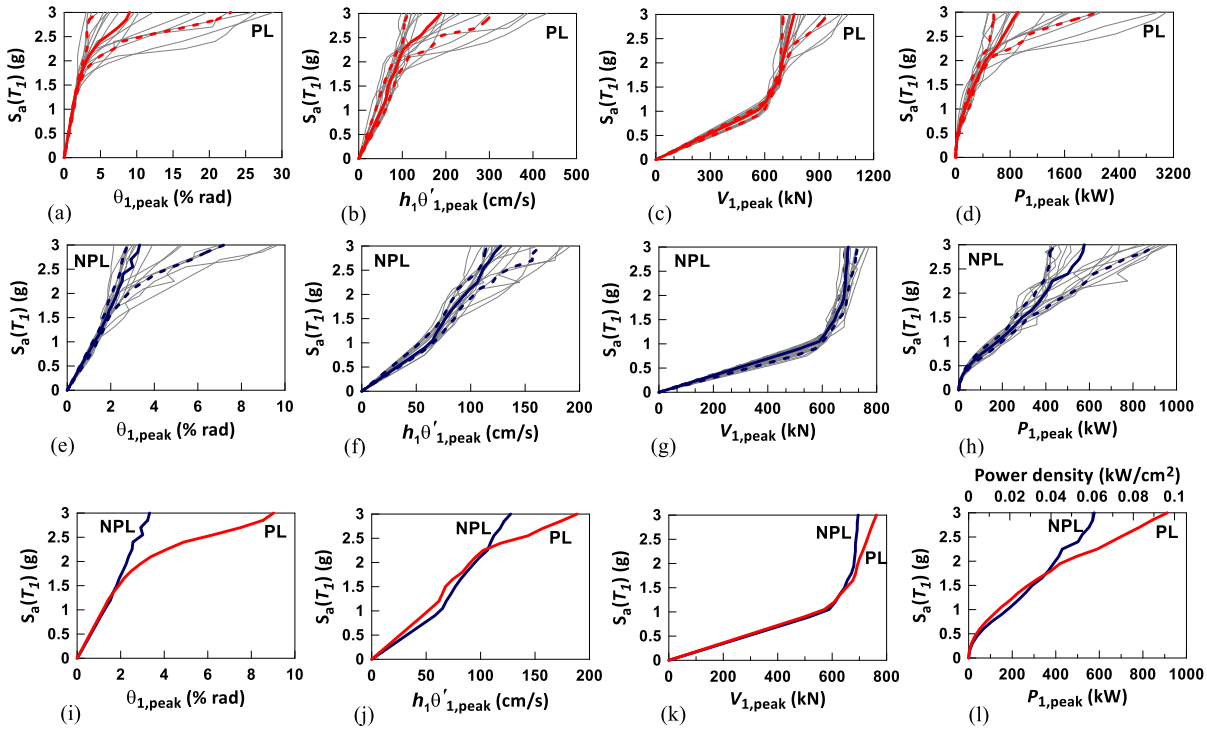

Figure 4. (a) $\theta_{1,peak}$, (b) $h_1\theta'_{1,peak}$, (c) $V_{1,peak}$, and (d) $P_{1,peak}$ IDA curves for the three-story building subjected to the PL ground motions. (e)–(h) are the counterparts of (a)–(d) subjected to the NPL ground motions. The medians of the (i) $\theta_{1,peak}$, (j) $h_1\theta'_{1,peak}$, (k) $V_{1,peak}$, and (l) $P_{1,peak}$ IDA curves for the three-story building subjected to the PL and NPL ground motions.

Conclusions

Pulse-like (PL) ground motions with prominent velocity pulses usually pose a severe risk to building structures. The present study suggests power demand as an alternative engineering demand parameter for reflecting the severity of the risk posed by PL ground motions. The proposed parameter is simply a product of story shears and inter-story velocities. Through an investigation using a three-story building subjected to ensembles of PL and non-pulse-like (NPL) ground motions, this study confirms that power demand satisfactorily elucidates the destructive potential of PL ground motions. In contrast, force demand, which is the cornerstone laid in building seismic design codes, cannot adequately reflect the destructive potential of PL ground motions.

Proceedings of the 2nd Croatian Conference on Earthquake Engineering - 2CroCEE
Zagreb, Croatia - March 22 to 24, 2023

DOI: https://doi.org/10.5592/CO/2CroCEE.2023.3

Acknowledgements

The author gratefully acknowledges Dr. Shu-Hsien Chao and Prof. Chun-Hsiang Kuo, colleagues at the National Center for Research on Earthquake Engineering, whose expertise is in seismic hazards and strong ground motions, for providing the ground motion record ensembles.

Appendix A

Fig. A1a–A1c shows the top view, front elevation, and side elevation of the three-story building. There is one bay in the x-direction and two bays in the y-direction of the building. The span of each bay is 350 cm. The walls are infilled only on the two exterior sides of the third story along the x-direction (Fig. A1c). The first story height, measured from the top of the pedestals (footings) to the top of the first floor slab, is 300 cm. The other story heights, measured from slab top to slab top, are 150 cm (Fig. A1b and A1c). The size of all beams is 25 cm × 40 cm. The size of the three columns in column line A, denoted by C2, is 75 cm × 30 cm, and the size of the three columns in column line B, denoted by C1, is 30 cm × 30 cm (Fig. A1a). Fig. A1d and A1e shows the details of the reinforcements for beams and columns. The materials used for the #3 (10ϕ) and #6 (19ϕ) reinforcements are SD280W and SD420W, respectively, and the nominal yielding strengths of these reinforcements are 280 MPa and 420 MPa, respectively. The 28-day compression strength of the concrete, denoted by f_c', is 21 MPa. According to the material tests on the reinforcements and concrete cylinders, the actual yielding strengths of the #3 and #6 reinforcements are 355 MPa and 454 MPa, respectively. In addition, the average 28-day compression strength is 21.96 MPa. The thickness of the slabs and walls are 10 cm and 15 cm, respectively. The details of the reinforcements for walls and slabs are #3@15 cm on two sides and in two directions. The size of each concrete pedestal is 75 cm (length) × 115 cm (width) × 70 cm (height). The pedestal is connected to a steel base plate with shear studs. The base plates are fixed to the shaking table by bolts (Fig. A1f). Two additional concrete mass blocks, each of which is 110 cm (length) × 110 cm (width) × 50 cm (height), are embedded in the second and third story slabs (Fig. A1a). Because the 50 cm height of the mass blocks is greater than the thickness of the slab (10 cm), the 30 cm and 10 cm heights of the mass blocks protrude from the bottom and top surfaces of the slabs, respectively. This three-story building was modularly constructed, using a combination of modules A, B, and C connected via steel connection plates (Fig. A1g). The vertical bars of the columns and walls were welded to steel connection plates. Consecutive modules were connected by having their respective steel plates bolted together (Fig. A1g). The resultant weight of the three-story building is 505 kN, which consists of 183.8 kN, 168.9 kN, and 152.3 kN for the first, second, and third stories, respectively.

Proceedings of the 2nd Croatian Conference on Earthquake Engineering - 2CroCEE
Zagreb, Croatia - March 22 to 24, 2023

DOI: https://doi.org/10.5592/CO/2CroCEE.2023.3

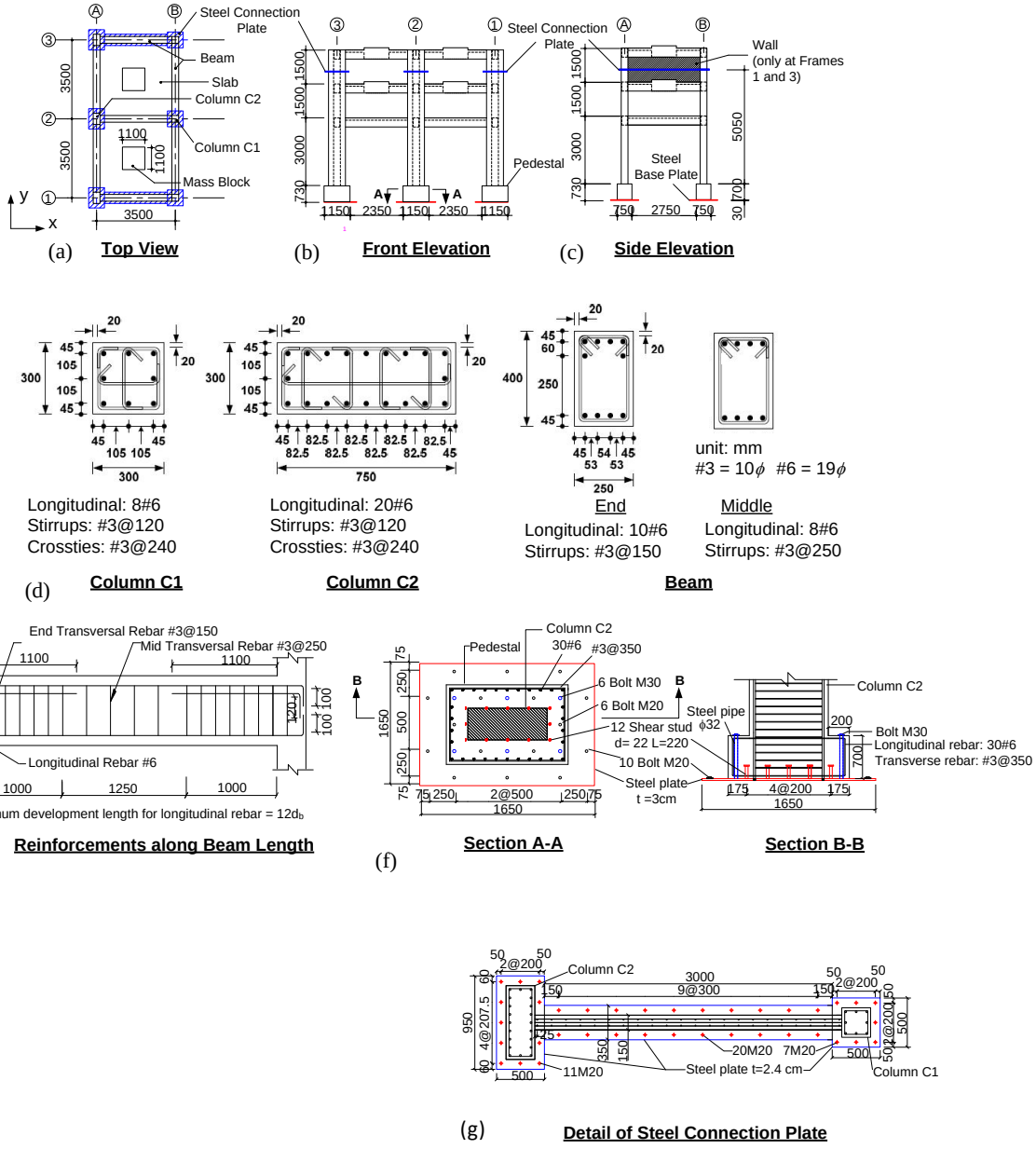

Figure A1. (a) Top view, (b) front elevation, and (c) side elevation of the three-story building; (d) cross sections of beams and columns; (e) reinforcements along beam length; (f) detail of the pedestal; and (g) detail of a steel connection plate.

References

[1] Bolt, B.A., Abrahamson, N.A. (2003): Estimation of strong seismic ground motions. *International Handbook of Earthquake and Engineering Seismology*, 81B, 983–1001.

[2] Mavroeidis, G.P., Papageorgiou, A.S. (2003): A mathematical representation of near-fault ground motions. *Bulletin of the Seismological Society of America*, **93**(3), 1099–1131.

[3] Bray, J.D., Rodriguez-Marek, A. (2004): Characterization of forward-directivity ground motions in the near-fault region. *Soil Dynamics and Earthquake Engineering*, **24**, 815–828.

[4] Kalkan, E., Kunnath, S.K. (2006): Effects of Fling Step and Forward Directivity on Seismic Response of Buildings. *Earthquake Spectra*, **22**(2), 367–390.

[5] International Conference of Building Officials (ICBO). *International Building Code*, Whittier, CA; 2000.

Proceedings of the 2nd Croatian Conference on Earthquake Engineering - 2CroCEE
Zagreb, Croatia - March 22 to 24, 2023

DOI: https://doi.org/10.5592/CO/2CroCEE.2023.3

[6] Sehhati, R., Rodriguez-Marek, A., ElGawady, M., Cofer, W.F. (2011): Effects of near-fault ground motions and equivalent pulses on multi-story structures. *Engineering Structures*, **33**, 767–779.

[7] Enderami, S.A., Beheshti-Aval, S.B., Saadeghvaziri, M.A. (2014): New energy based approach to predict seismic demands of steel moment resisting frames subjected to near-fault ground motions. *Engineering Structures*, **72**: 182–192.

[8] Kalkan, E., Kunnath, S.K. (2007): Effective cyclic energy as a measure of seismic demand. *Journal of Earthquake Engineering*, **11**(5), 725–751.

[9] Lin, J.L., Chen, W.H., Hsiao, F.P., Weng, Y.T., Shen, W.C., Weng, P.W., Li, Y.A., Chao, S.H. (2020): Simulation and analysis of a vertically irregular building subjected to near-fault ground motions. *Earthquake Spectra*, **36**(3), 1485–1516.

[10] Shahi, S.K., Baker, J.W. (2014): An efficient algorithm to identify strong-velocity pulse in multicomponent ground motions. *Bulletin of the Seismological Society of America*, **104**(5), 2456–2466.

[11] Vamvatisikos, D., Cornell, C.A. (2002): Incremental dynamic analysis. *Earthquake Engineering and Structural Dynamics*, **31**, 491–514.